Effects of nonequilibrium quasiparticles in a thin-film superconducting microwave resonator under optical illumination

R. P. Budoyo, J. B. Hertzberg, C. J. Ballard, K. D. Voigt, Z. Kim, J. R. Anderson, C. J. Lobb, and F. C. Wellstood

Effects of Nonequilibrium Quasiparticles in a Thin-Film Superconducting Microwave Resonator under Optical Illumination

R. P. Budoyo,* J. B. Hertzberg,† C. J. Ballard, K. D. Voigt, Z. Kim,‡ J. R. Anderson, C. J. Lobb, and F. C. Wellstood

Joint Quantum Institute and Center for Nanophysics and Advanced Materials,
Department of Physics, University of Maryland, College Park, Maryland, 20742 USA

We have illuminated a thin-film superconducting Al lumped-element microwave resonator with 780 nm light and observed the resonator quality factor and resonance frequency as a function of illumination and microwave power in the 20 to 300 mK temperature range. The optically-induced microwave loss increases with increasing illumination but decreases with increasing microwave power. Although this behavior may suggest the presence of optically activated two-level systems, we find that the loss is better explained by the presence of nonequilibrium quasiparticles generated by the illumination and excited by the microwave drive. We model the system by assuming that the illumination creates an effective source of phonons with energy higher than double the superconducting gap and solve the coupled quasiparticle-phonon rate equations. We fit the simulation results to our measurements and find good agreement with the observed dependence of the resonator quality factor and frequency shift on temperature, microwave power, and optical illumination. Examination of the model reveals approaches to reducing optically-induced loss and improving the relaxation time of superconducting quantum devices.

I. INTRODUCTION

Superconducting materials that are cooled far below their transition temperature T_c can exhibit very low levels of dissipation at microwave frequencies. Although the remaining dissipation can be very small, it can still limit the lifetime of superconducting qubits[1,2] and the performance of microfabricated superconducting resonators[3,4] and kinetic-inductance radiation detectors[5,6] operating in the 0.01 K to 1 K temperature range.

Over the last decade, a range of devices and materials have been explored to understand what is causing the residual loss. This has yielded dramatic reductions in loss and three main physical mechanisms have been identified. First, coupling to bias lines or other microwave modes can cause loss that is independent of rf power. Second, charged two-level systems (TLSs) present in dielectric regions can couple to a device's electric field, causing loss. TLS loss exhibits a distinct power-dependent saturation behavior[3,7,8] that leads to a characteristic decrease in loss with an increase in temperature or microwave power. Third, dissipation can be caused by quasiparticles which can be created by thermal effects, stray light, radiation, or other mechanisms[9–15]. Quasiparticle generation from ionizing radiation or photons provides the physical basis for superconducting radiation detectors[5,6,10,14], and is also relevant to some proposed hybrid quantum systems in which a superconducting device must function in close proximity to optically trapped atoms[16,17]. There has also been renewed interest in the role of quasiparticles as a loss and decoherence mechanism in superconducting qubits[18–20]. Although qubits operate at the single-photon level, there is also interest in applying high rf powers to qubits and their readout resonators for both readout[21] and gate coupling[22].

In this work, we report measurements on a lumped-element superconducting microwave resonator that is embedded in a 3D cavity with extremely weak coupling to the fundamental mode of the cavity. This arrangement is similar to that used in 3D transmons[23]. Illuminating the resonator with optical photons, we observe a decrease in its resonance frequency and an increase in loss. We find that this photo-induced loss decreases with increasing rf drive, much as one expects for loss from coupling to an ensemble of TLSs[24]. However, we argue below that the power-dependent loss is actually due to the subtle behavior of nonequilibrium quasiparticles[13]. We discuss modelling of the power-dependent optically-induced loss and resonator frequency shift as a function of temperature, optical power, and rf power. Comparing our results to those expected from TLSs and to those expected from quasiparticles, we conclude that the data are better explained by nonequilibrium quasiparticles. Finally, we examine some of the factors in the model that affect the loss, and suggest approaches for reducing it.

II. LOSS FROM TWO-LEVEL SYSTEMS

The internal quality factor Q_i of a superconducting microwave resonator can be found from

$$Q_i^{-1} = Q_{\text{TLS}}^{-1} + Q_{qp}^{-1} + Q_0^{-1}, \tag{1}$$

where Q_{TLS} is the quality factor from two-level systems in the dielectric regions of the resonator, Q_{qp} is the quality factor from quasiparticles, and Q_0 is the power-independent quality factor from coupling to other microwave modes or other loss channels.

The inverse quality factor at frequency f_r produced by an ensemble of TLSs can be written as[7,24]

$$Q_{\text{TLS}}^{-1} = \frac{F \tan(\delta) \tanh(hf_r/2k_bT)}{\sqrt{1 + (V_{\text{rms}}/V_c)^2}}, \tag{2}$$

where F is the resonator's dielectric fill factor, $\tan(\delta)$ is the dielectric loss tangent, T is the temperature, V_{rms}

is the rms voltage across the capacitor at frequency f_r, and V_c is the characteristic saturation voltage for the TLSs in the dielectric. V_{rms}^2 is proportional to the rf drive power P_{rf}, and thus Eq. (2) shows decreasing loss with increasing power. Eq. (2) also yields TLS loss that decreases with increasing temperature. These dependences of the loss on power and temperature have been used as qualitative and quantitative signatures to distinguish TLS loss from other mechanisms. While significant deviations from Eq. (2) have been observed[25,26], these have been understood to arise from TLS interactions[27,28] or a distribution of TLS dipole moments[29].

One expects that optical illumination would increase the effective temperature of the TLSs, as has been reported, for example, for Nb on Si resonators under 635 nm illumination[30]. Increased temperature would reduce the TLS-induced loss due to the tanh factor in Eq. (2). One might also expect that photoabsorption could activate a TLS that was otherwise not contributing to the loss. However, photoabsorption could also remove TLSs from the bandwidth of the resonator, leading to reduced loss. Since the TLS asymmetry energy is expected to be uniformly distributed[24], we would not expect photoabsorption to produce a net change in the number of active TLSs in the bandwidth of the resonator. Thus, the net effect of optical illumination should be to reduce the TLS loss.

III. LOSS FROM NONEQUILIBRIUM DISTRIBUTION OF QUASIPARTICLES

To find the expected rf loss produced by quasiparticles, we will need to find the distribution of quasiparticles $f(E)$ as a function of the quasiparticle energy E, the rf power, the optical power, and the temperature. We will also need to find the distribution of phonons $n(\Omega)$ as a function of the phonon energy Ω because quasiparticles can change energy by emitting and absorbing phonons, and the rate depends on the phonon distribution. To model the effect of light being absorbed in the superconductor, we include optically-induced pair-breaking in the simulation.

Goldie and Withington have described a numerical procedure for finding $f(E)$ and $n(\Omega)$ in a superconductor under a microwave drive[31] using a set of kinetic equations initially derived by Chang and Scalapino[32] (see Appendix). With Guruswamy, they have extended their approach[33,34] to include effects of pair breaking for photons with energies up to about 10Δ, where Δ is the superconducting gap. However, in our case we used optical photons with an energy of approximately 1.6 eV $\approx 9000\Delta$. For such energetic photons the effects on the superconductor are similar to adding a source of hot phonons[9,34–36]. Accordingly, we extend Goldie et al.'s approach by using a heating model that accounts for optical radiation by introducing a phonon generating term with an effective temperature T_{eff} determined by the op-
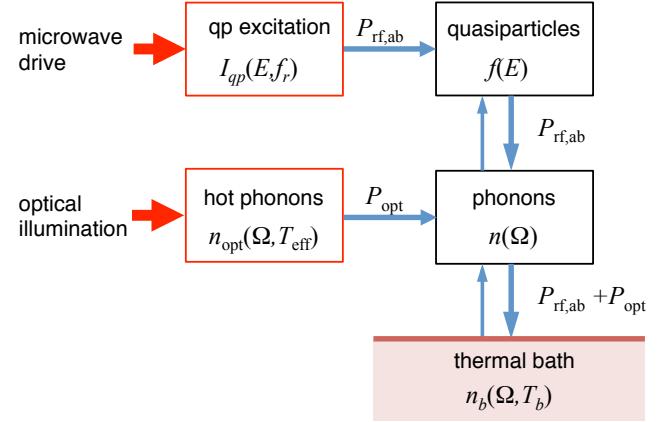
FIG. 1. Diagram showing model for steady-state power flow in the quasiparticles and phonons in a thin-film superconducting resonator under optical illumination.

tical power.

Figure 1 shows the thermal model of our system. Microwave power $P_{rf,ab}$ is absorbed by the quasiparticles, which can exchange energy with a bath of phonons with distribution $n(\Omega)$. The phonons are also connected to a thermal bath and an effective hot phonon source that accounts for optical absorption. As described by Chang and Scalapino[32], the absorbed optical power P_{opt} acts as an additional phonon generating source term

$$\frac{dn(\Omega)}{dt}\bigg|_{opt} = \frac{n_{opt}(\Omega, T_{eff})}{\tau_e}. \tag{3}$$

Here τ_e is the escape time for phonons to leave the superconductor and go into the substrate[37]. We use a version of the Parker heating model[35] and set

$$n_{opt}(\Omega, T_{eff}) = \begin{cases} 0, & \text{for } \Omega < 2\Delta \\ 1/(e^{\Omega/k_B T_{eff}} - 1), & \text{for } \Omega > 2\Delta, \end{cases} \tag{4}$$

Although n_{opt} takes the form of a Bose-Einstein thermal distribution with effective temperature T_{eff} for $\Omega > 2\Delta$, it is not a thermal distribution since $n_{opt} = 0$ for $\Omega < 2\Delta$.

To use Eq. (4) we need to establish a connection between T_{eff} and the absorbed optical power P_{opt}. Considering the steady state power flow in the system (see Fig. 1), the optical power P_{opt} transferred to the phonon distribution $n(\Omega)$ by n_{opt} is

$$P_{opt}(T_{eff}) = V \int_0^\infty d\Omega \, D(\Omega) \, \Omega \, \frac{n_{opt}(\Omega, T_{eff})}{\tau_e}, \tag{5}$$

where $D(\Omega) = 9N_i\Omega^2/\Omega_D^3$ is the phonon density of states, N_i is the atomic density of Al, V is the volume of Al in the resonator, and Ω_D is the Debye energy for aluminum. Assuming the light is perpendicularly incident on the superconductor, the absorbed optical power is

$$P_{opt} = \epsilon I_{opt} A, \tag{6}$$

where ϵ is the emissivity of the aluminum film, I_{opt} is the incident optical intensity, and A is the illuminated area of the resonator.

To find the microwave loss from $f(E)$, we note that the complex conductivity of the superconductor is $\sigma = \sigma_1 - i\sigma_2$ and for frequencies $f_r < 2\Delta/h$ is given by[38]

$$\frac{\sigma_1(f_r)}{\sigma_n} = \frac{2}{hf_r} \int_{\Delta}^{\infty} dE \left[f(E) - f(E + hf_r) \right] \rho(E) \\ \times h_+(E, E + hf_r), \tag{7}$$

$$\frac{\sigma_2(f_r)}{\sigma_n} = \frac{1}{hf_r} \int_{\Delta - hf_r}^{\Delta} dE \left[1 - 2f(E + hf_r) \right] \frac{E}{\sqrt{\Delta^2 - E^2}} \\ \times h_+(E, E + hf_r), \tag{8}$$

where σ_n is the conductivity of the normal state, the coherence factors h_+ and h_- are given by

$$h_\pm(E, E') \equiv \left(1 \pm \frac{\Delta^2}{EE'} \right) \rho(E'), \tag{9}$$

and $\rho(E) = E/\sqrt{E^2 - \Delta^2}$ is the normalized density of states of the quasiparticles. From σ, we obtain[9]

$$Q_{qp}^{-1} = \alpha_1 \sigma_1/\sigma_2, \tag{10}$$

and the fractional frequency shift in the resonance frequency

$$\delta f_r/f_r = \alpha_2 \delta\sigma_2/2\sigma_2, \tag{11}$$

where $\delta\sigma_2 = \sigma_2 - \sigma_{2,0}$ and $\sigma_{2,0}$ is the imaginary part of σ for $I_{\mathrm{opt}} = 0$, rf drive power $P_{\mathrm{rf}} = 0$, and bath temperature $T_b = 0$. α_1 and α_2 are scaling factors that are expected to be equal to the kinetic inductance ratio $L_k/(L_k + L)$, where L_k is the kinetic inductance of the resonator, and L the geometric inductance of the resonator[39].

Some general remarks can be made about the solutions. Without optical illumination ($P_{\mathrm{opt}} = 0$), de Visser et al. have shown[13] that the loss from quasiparticles depends on the rf drive power P_{rf} and the bath temperature T_b. In Al below about 200 mK, they reported that the loss increases with increasing drive, but at higher temperatures the loss decreases with increasing drive. With increasing optical illumination, we find the loss increases as expected due to an increased number of quasiparticles. We also find that this optically-induced loss decreases with increasing microwave drive within the range of rf powers and optical intensities that we used in our experiments. The reason for this behavior is similar to the higher temperature case described by de Visser et al.[13]. In this regime the rf drive causes a redistribution of the quasiparticles such that $f(E)$ increases for $E \geq \Delta + hf_r$ and decreases for $\Delta \leq E \leq \Delta + hf_r$. This causes a decrease in the term $f(E) - f(E + hf_r)$ in Eq. (7) which in turn causes σ_1 and $1/Q_{qp}$ to decrease.

IV. EXPERIMENTAL SETUP

Figure 2 shows our experimental setup. The resonator [see Fig. 2(a)] is about 0.4 mm on a side and has an
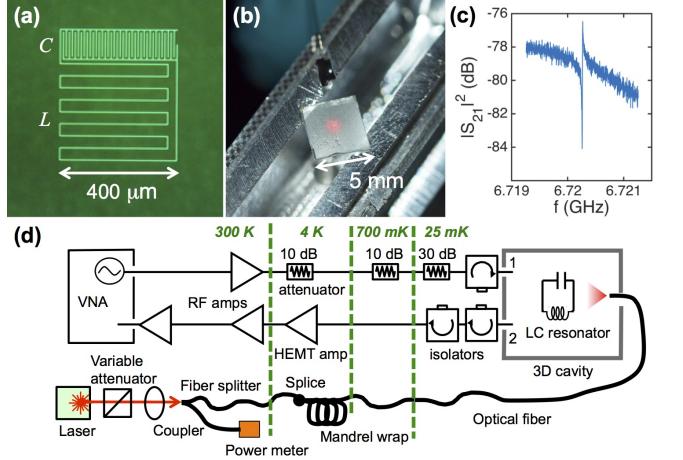
FIG. 2. (a) Photograph of lumped-element resonator made from 215 nm thick Al film showing meandering inductor L and interdigitated capacitor C. (b) Photograph of resonator chip mounted in cavity, illuminated by light (red spot) supplied by optical fiber in bottom of the cavity. (c) Transmission $|S_{21}|^2$ vs frequency showing LC resonance at $f = 6.720$ GHz. (d) Schematic of measurement setup showing microwave drive line between VNA and port 1 of 3D cavity, the LC resonator, microwave readout line between port 2 of 3D cavity and VNA, and the 780 nm illumination line.

interdigitated capacitor with capacitance $C \approx 150$ fF and a meandering inductor with inductance $L \approx 3.5$ nH, similar to resonators used for reading out single-electron transistors[40] and for circuit QED read-out of qubits[41]. To build the device, a 215 nm Al layer was thermally-evaporated onto a sapphire chip, patterned using optical lithography and wet etched. The same design was used in other work[42], except here we used a second wet etch to remove an input/output transmission line and ground plane, leaving just an isolated LC resonator on an otherwise bare sapphire chip. The resonant frequency at 25 mK was $f_r = 1/2\pi\sqrt{LC} = 6.720$ GHz. The dilution refrigerator was thermally cycled above 1.5 K several times during the measurements and we found that the resonance frequency shifted by up to 50 kHz between cycles.

The chip was mounted into the center of a microwave cavity [see Fig. 2(b)] that was machined from Al 6061 alloy and had a TE101 mode frequency of 7.50 GHz. This arrangement provided an extremely weak coupling of the LC resonator to the output (port 2) and input (port 1) lines, giving $Q_e \approx 4.9 \times 10^9$. Because of the 780 MHz detuning between the cavity resonance and LC resonance, and the extremely small coupling between them, we can treat the LC and the cavity resonances as effectively independent.

To illuminate the LC resonator, we used a diode laser emitting 780 nm light, a wavelength suitable for hybrid quantum systems employing optically trapped ^{87}Rb atoms[16,17]. Light was carried to the device via a single-mode optical fiber [see Fig. 2(d)]. The power coupled into the fiber was measured using a power meter connected to

one arm of a 50-50 fiber splitter. At the 4 K stage, the fiber was wrapped about 20 times around a 2.5 cm post to suppress multi-mode transmission in the fiber jacket. The end of the fiber was epoxied into a hole in the bottom of the cavity about 1 cm below the chip.[43] The cone of light illuminating the chip surface was about 1.4 mm in diameter, centered on the LC resonator [see Fig. 2(b)].

The range of incident optical intensities used was $I_{\mathrm{opt}} = 20$ to 812 aW/μm^2 at the chip surface. This corresponds to roughly 80 to 3200 optical photons per second per μm^2 striking the Al surface of the LC resonator. The total surface area of the resonator's Al was $A \approx 4.18 \times 10^4 \mu$m^2, which gave an incident power range of 0.83 to 34 pW. As expected, no significant effect on the temperature of the refrigerator was observed at these small power levels.

The cavity was mounted on the mixing chamber stage of an Oxford Instruments cryogen-free dilution refrigerator. The cavity's input and output microwave lines were well-isolated from thermal noise from higher temperature stages by the placement of microwave attenuators on the input line and microwave isolators at the output line. We used an Agilent E5071C Vector Network Analyzer (VNA) to measure the S_{21} of the LC resonance [see Fig. 2(c)]. We fit the in-phase and quadrature components of the frequency-dependent background S_{21} to a 4th-order polynomial and subtracted this background. The applied rf power P_{rf} is defined as the power at the input port 1 of the cavity. For lower P_{rf} values, the LC resonance frequency f_r and Q were obtained from a simultaneous fit of the real and imaginary components of S_{21} to a Lorentzian. For higher P_{rf} values, where strong dependence of Q on P_{rf} caused the resonance shape to deviate from Lorentzian, we used the measured resonance peak amplitude to infer Q/Q_e.

The maximum rf power we applied at the input of the cavity depended on the temperature and optical intensity. At low temperatures and low optical intensities, the resonance peak showed switching behavior at high rf powers due to nonlinear effects[44,45]. The power level where this behavior appeared was at $P_{\mathrm{rf}} \approx -45$ dBm when $I_{\mathrm{opt}} = 0$, and increased with I_{opt}. For higher optical intensities, the upper limit was around $P_{\mathrm{rf}} \approx -40$ dBm due to the compression point of our amplifiers. At higher temperatures (above about 230 mK), the resonator appeared to self-heat when driven continuously above $P_{\mathrm{rf}} \approx -55$ dBm, and this determined the upper limit for the measurement power. We focused our measurements on rf drive powers P_{rf} greater than -70 dBm, which corresponds to about 5×10^4 rf photons in the resonator at 25 mK. For P_{rf} values below -70 dBm, there was a significant decrease in Q that we attributed to TLS loss and the resonance frequency occasionally jumped between different branches, suggesting strong coupling to an individual TLS[46].
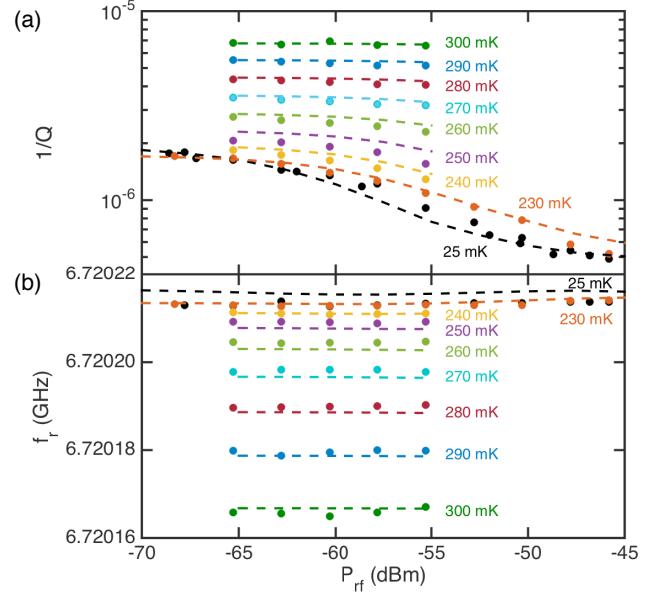
FIG. 3. (a) Inverse quality factor $1/Q$ and (b) resonance frequency f_r of the LC resonator vs applied rf power P_{rf} (measured at the cavity input) at listed temperatures T with no illumination. Filled circles are data. Dashed curves were calculated from the nonequilibrium simulation with a background illumination giving an effective phonon source temperature $T_{\mathrm{eff}} = 236$ mK.

V. QUALITY FACTOR AND FREQUENCY SHIFT AT HIGHER TEMPERATURES, NO ILLUMINATION

The filled circles in Fig. 3 show measured results for $1/Q$ and f_r as a function of P_{rf} for different temperatures for no optical power applied by the fiber. The results shown for 25 mK were averaged from multiple measurements for the same P_{rf}. We found that Q and f_r showed negligible temperature dependence between 25 mK and 230 mK when no optical power was applied.

For comparison, the dashed curves in Fig. 3 show best fit results for $1/Q$ and f_r from the nonequilibrium model. In the simulation, we assume initial values for all of the model parameters (see Table I), including I_{opt}, P_{rf}, and T_b. We follow the numerical procedure described by Goldie and Withington[31] (see Appendix) to solve $f(E)$ and $n(\Omega)$ for the steady state condition $df(E)/dt = 0$ and $dn(\Omega)/dt = 0$. From $f(E)$ we find σ_1, σ_2 using Eqs. (7) and (8) and then use Eqs. (10) and (11) to find Q_{qp}^{-1} and $\delta f_r/f_r$. We repeat the process for a range of P_{rf}, T, and I_{opt}, and then compare the results to our measured value of $1/Q$ and $\delta f_r/f_r$. We adjust the parameters and repeat the entire process to fit the model to the entire data set of Q and $\delta f_r/f_r$ vs P_{rf}, I_{opt}, and T.

The parameters used in the simulation are shown in Table I. We set $1/Q_{\mathrm{TLS}} = 0$ due to the expected saturation at higher drive powers but included a constant loss term by setting $1/Q_0 \approx 2.5 \times 10^{-7}$. For these fit curves,

TABLE I. Parameters used in the nonequilibrium simulations

Symbol	Parameter	Value	Source
Δ	superconducting gap	167 μeV	fit parameter
f_r	rf drive frequency in simulation	28 μeV$/h$	closest 1 μeV$/h$ multiple
		(= 6.770 GHz)	to drive frequency
A	resonator Al surface area	$4.18 \times 10^4 \mu$m^2	design value
V	resonator Al volume	$8.99 \times 10^3 \mu$m^3	design value
Q_e	external quality factor of LC resonator	4.9×10^9	fit to S_{21}
N_0	single-spin density of states at Fermi level	1.74×10^{10} eV$^{-1}\mu$m^{-3}	Ref. [31]
N_i/Ω_D^3	atom density/(Debye energy)^3	1.41×10^{15} (eV μm)$^{-3}$	Eq. (A.6)
τ_0	quasiparticle-phonon scattering time	438 ns	Ref. [47]
τ_ϕ	phonon-quasiparticle scattering time	0.26 ns	Ref. [31]
τ_e	phonon escape time	8.96 ns	Eqs. (5) and (6)
ϵ	optical absorption coefficient of Al	$\approx 15\%$	nominal
$1/Q_{\mathrm{TLS}}$	TLS loss component	0	nominal
$1/Q_0$	power independent loss component	2.5×10^{-7}	fit parameter
α_1	$1/Q$ scaling factor in Eq. (10)	0.61%	fit parameter
α_2	$\delta f_r/f_r$ scaling factor in Eq. (11)	0.88%	fit parameter
f_0	baseline LC resonator frequency	6.720225 GHz	fit parameter
$T_{\mathrm{eff},0}$	effective temperature of background radiation	236 mK	fit parameter

we had to set $T_{\mathrm{eff}} = 236$ mK corresponding to a background illumination. Overall the simulation captures the behavior of $1/Q$ and f_r with changing rf drive and temperature, although there are small discrepancies between the simulation and data in particular in the $240 - 260$ mK range. This discrepancy may be due to approximations inherent in our model for n_{opt} or the background illumination.

To illustrate the behavior of the solutions, the solid curves in Fig. 4 show the quasiparticle distributions $f(E)$ and phonon distributions $n(\Omega)$ as a function of normalized energy for $T_b = 25$ mK and optical illumination producing $T_{\mathrm{eff}} = 236$ mK for several values of P_{rf}. These are clearly nonequilibrium distributions with peaks appearing at energies hf_r apart due to the microwave drive term. There are also jumps in $f(E)$ at $E = 3\Delta$ and in $n(\Omega)$ at $\Omega = 2\Delta$. These come from the discontinuity in n_{opt} as well as pair breaking and recombination. $f(E)$ generally increases with increasing P_{rf}, except near $E = \Delta$ where it decreases instead [see Fig. 4(c)]. It is this decrease that causes $1/Q_{qp}$ to decrease with increasing rf drive power P_{rf}. For comparison, the dashed green curves in Fig. 4 show $f(E)$ and $n(\Omega)$ for a thermal distribution with $T = 236$ mK. Although this is a very coarse log scale, the nonequilibrium $n(\Omega)$ distributions roughly follow the thermal distribution for $\Omega > 2\Delta$, as would be expected due to the n_{opt} source term.

The fact that the effective temperature with no optical illumination ($T_{\mathrm{eff},0} = 236$ mK) is much higher than the refrigerator's base temperature of 25 mK suggests the presence of significant background radiation. This may have been due to radiation from a hot finger that was anchored at 4 K, and extended to within a few inches
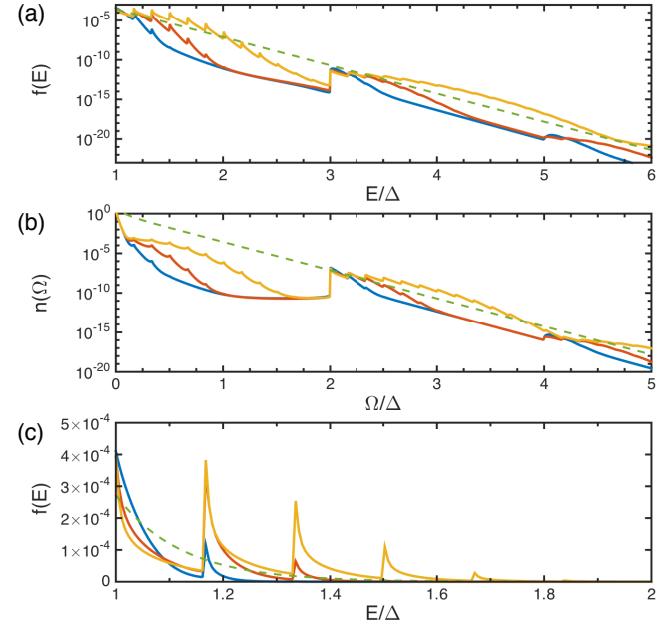
FIG. 4. (a) Simulated quasiparticle distribution $f(E)$ as a function of normalized quasiparticle energy E/Δ for three drive powers P_{rf}, with $T_b = 25$ mK and $T_{\mathrm{eff}} = 236$ mK. Blue is for $P_{\mathrm{rf}} = -65$ dBm, red is for $P_{\mathrm{rf}} = -55$ dBm, and yellow is for $P_{\mathrm{rf}} = -45$ dBm. For comparison, green dashed curve shows the Fermi-Dirac distribution at 236 mK. (b) Simulated phonon distribution $n(\Omega)$ as a function of normalized phonon energy Ω/Δ. Green dashed curve is the Bose-Einstein distribution at 236 mK. Other colored curves are for the same rf powers as in (a). (c) Detailed view of (a) for E between Δ and 2Δ.
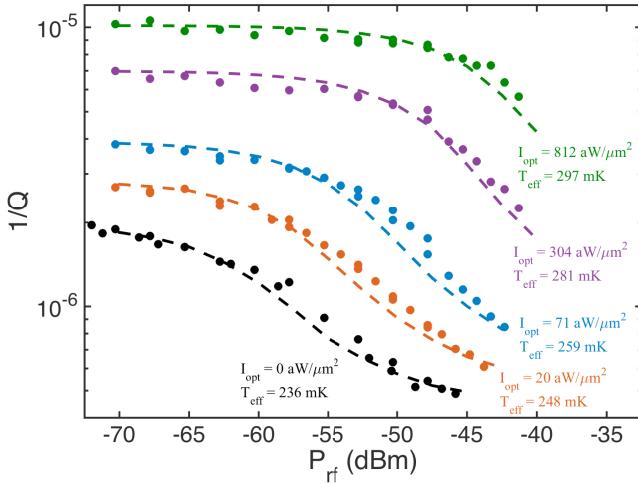
FIG. 5. Inverse quality factor $1/Q$ of resonator as a function of applied rf power P_{rf} for different illumination intensities I_{opt} at base temperature. Closed circles are data and dashed curves were found from the nonequilibrium simulation with $T_b = 25$ mK. For each optical intensity, the effective temperature T_{eff} was varied in the simulation to find the best fit.

of the cavity. This hot finger was used in a separate experiment in the same cooldown and also caused the refrigerator base temperature to increase from 10 mK to 25 mK.

We can approximate the effect of a 4 K source on the cavity using the Parker heating model. We assume the ballistic phonon limit where τ_e is proportional to thickness[37] and assume the volume of Al forming the cavity is proportional to the illuminated area. With these assumptions, Eq. (5) yields an effective temperature that is independent of the cavity dimensions. Using $I_{\text{opt}} = 15$ aW/μm^2 for black-body radiation from the 4 K hot finger we find the effective temperature of the radiation heating the cavity to be $T_{\text{eff,c}} \approx 231$ mK, which is close to the value from our fit to the data. This suggests the hot finger caused a nonequilibrium distribution of phonons in the cavity and the enclosed resonator.

VI. QUALITY FACTOR AND FREQUENCY SHIFT UNDER ILLUMINATION

Figure 5 shows a plot of the resonator's inverse quality factor $1/Q$ as a function of P_{rf} for five different optical illuminations. We note that for all illuminations, $1/Q$ decreases with increasing rf power, with a shape that is similar qualitatively to what Eq. (2) predicts for loss from a TLS bath. The P_{rf} values where $1/Q$ starts decreasing rapidly increases with increasing I_{opt}, but our analysis reveals that this onset appears when the rms voltage across the capacitor $V \approx 10$ mV in all the curves. This behavior may again suggest loss from a TLS bath, however a critical voltage value of $V_c = 10$ mV would correspond to $n_c \sim 10^6$ microwave photons in the resonator. Both V_c

and n_c are much larger than typical for TLS loss. From previous measurements of Al resonators with comparable size and frequency[4,19,48], we expect $n_c \approx 1 - 100$ and our high value would require a very small TLS dipole moment or a very short TLS lifetime. Furthermore, as discussed above we expect the loss from a TLS bath to decrease with increasing optical intensity and we are not aware of a mechanism that produces an increase in TLS loss under illumination. Examination of the data reveals that the loss increases with illumination as approximately $I_{\text{opt}}^{1/2}$. This is the expected dependence for the number of quasiparticles generated by pair breaking radiation in the steady state[49], which suggests that the increased loss is due to quasiparticles rather than TLSs.

As shown by the dashed curves in Fig. 5, for the entire range of intensities we find remarkably good agreement between the data and fits from the non-equilibrium quasi-particles simulation. For these fit curves, we only varied T_{eff} and fixed $T_b = 25$ mK, $1/Q_0 = 2.5 \times 10^{-7}$, and all of the other parameters (see Table I). The range of T_{eff} is between 236 mK and 297 mK.

After fitting to the data shown in Figs. 3 and 5 all of the model parameters have been determined (see Table I). Considering the best fit parameters, the superconducting gap $\Delta = 167$ μeV is close to the expected value of the superconducting gap in Al of 170 μeV. The phonon escape time $\tau_e = 8.96$ ns $= 34\tau_\phi$ was set to maintain power balance for the absorbed optical power for $\epsilon \approx 15\%$. This value is about an order of magnitude larger than the equivalent value used by Goldie and Withington[31] and de Visser et al.[13], however it is within the range of reported values for τ_e for Al on sapphire[37]. We found that relatively large changes in τ_e resulted in relatively small changes in σ_1 and σ_2. We also note that both α_1 and α_2 are slightly less than 1%. This is consistent with our rough estimate of the kinetic inductance ratio of 1 to 1.5%[39].

In Fig. 6(a) we plot T_{eff} as a function of I_{opt}. The circles are from fits to our $1/Q$ vs P_{rf} data (see Fig. 5 for example). For comparison we assume that the total optical power is from the fiber and a background source. The solid curve is a fit of the circles to the expression

$$P_{\text{opt}}(T_{\text{eff}}) = P_{\text{opt}}(T_{\text{eff,0}}) + \gamma I_{\text{opt}}, \qquad (12)$$

where P_{opt} is numerically calculated from Eq. (5), while $T_{\text{eff,0}}$ and γ are fit parameters. We find excellent agreement between data and simulation with $T_{\text{eff,0}} = 238$ mK and $\gamma \approx 6.8 \times 10^3$ μm^2. From Eq. (6), we expect $\gamma = \epsilon A = 6.3 \times 10^3$ μm^2. The 10% discrepancy between the expected and the fit values of γ is less than the uncertainties in the surface emissivity ϵ and the incident optical intensity I_{opt}.

In Fig. 6(b) we compare the measured and simulated $1/Q$ values as a function of I_{opt} for $P_{\text{rf}} = -65$ dBm and -45 dBm. For the nonequilibrium simulation, we used $T_b = 25$ mK and T_{eff} values obtained from the fit shown in Fig. 6(a). For each P_{rf} we simulated $1/Q$ only for the nine I_{opt} values where we had data and performed
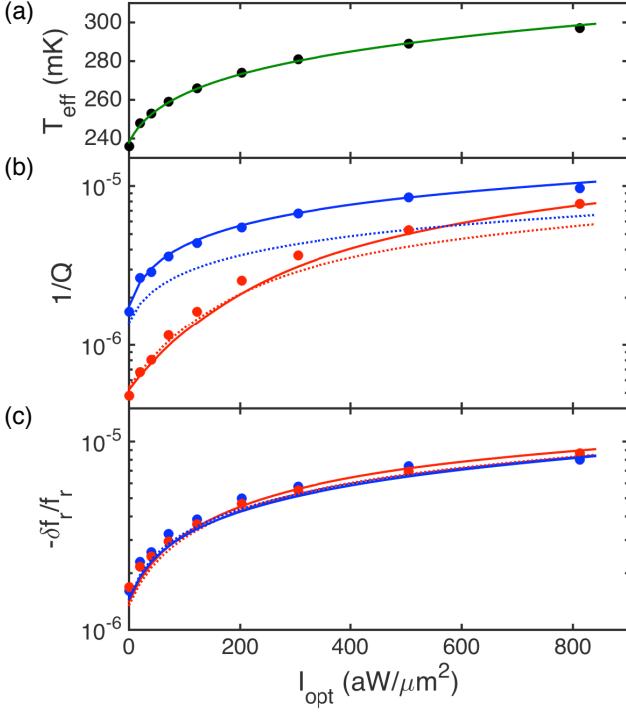
FIG. 6. (a) Effective temperature T_{eff} as a function of optical illumination intensity I_{opt}. Each closed black circle is extracted from a fit to the $1/Q$ vs P_{rf} data, as in Fig. 5. The green curve is a fit of the circles to Eq. (12). (b) Inverse quality factor $1/Q$ and (c) fractional frequency shift $-\delta f_r/f_r$ as a function of I_{opt} for $P_{\mathrm{rf}} = -65$ dBm (blue) and -45 dBm (red). In each plot, the closed circles are measured and the solid curves are from the nonequilibrium simulation with $T_b = 25$ mK and using the T_{eff} fit values shown in (a). For comparison, the dotted curves are from the nonequilibrium simulation assuming simple heating with $T_b = T_{\mathrm{eff}}$ from fit in (a) and no illumination ($P_{\mathrm{opt}} = 0$).

spline interpolation for other values of I_{opt}. There were no additional fit parameters. The data and simulation agree well for both P_{rf} values.

Illumination also caused a shift in the resonance frequency of the resonator. In Fig. 6(c) we compare the measured and simulated $\delta f_r/f_r$ values. The difference between the $P_{\mathrm{rf}} = -65$ dBm and $P_{\mathrm{rf}} = -45$ dBm curves is very small, and the data and simulation agree well. Given that this comparison involves no additional fit parameters, the good agreement is strong support for the loss being due to nonequilibrium quasiparticles. In effect we have used the resonator loss to predict the frequency shift.

VII. COMPARISON BETWEEN OPTICAL ILLUMINATION AND INCREASED TEMPERATURE

The simulations are complicated and require many input parameters. This raises the question of whether the

behavior can be captured with a simpler model. Gao *et al.* have suggested that pair-breaking radiation produces nearly the same effect on $1/Q$ and f_r as an increase in temperature[9].

In Fig. 6(b) and (c) we show a comparison between this increased temperature model (dashed curves) and our optical illumination model (solid curves). For the increased temperature model we assumed T_b values equal to the T_{eff} fit values in Fig. 6(a). The discrepancy in $\delta f_r/f_r$ between the two models is very small for both values of P_{rf}, as shown in Fig. 6(c). On the other hand, Fig. 6(b) shows that for $P_{\mathrm{rf}} = -65$ dBm the $1/Q$ from the temperature model is smaller than that from the data and the full model for the entire range of I_{opt}. For $P_{\mathrm{rf}} = -45$ dBm, the difference between the two models is negligible below $I_{\mathrm{opt}} \approx 300$ aW/μm^2, while for higher intensities the $1/Q$ from the increased temperature model yields significantly smaller values of $1/Q$ than we measure. This suggests that the non-equilibrium model for n_{opt} is better than the increased temperature model for simulating effects produced by optical illumination.

VIII. CONCLUSION

In conclusion, we illuminated a thin-film superconducting Al lumped-element resonator with 780 nm light and found loss that increased with illumination, but decreased with increasing rf drive power. While this behavior mimicked the behavior of optically activated two-level systems, it is well-explained by the physics of nonequilibrium quasiparticles that are generated by the illumination and excited by the rf drive. We observed a strong background radiation that we attributed to the presence of a 4 K hot finger near the cavity. We note that measurements of the rf-dependence of the photo-induced loss could be used to discriminate quasiparticle loss from TLS induced loss, confirm optical absorption in a resonator, detect nonequilibrium quasiparticles, and study quasiparticle dynamics at high rf-drive.

Examination of the kinetic equations suggest several methods for reducing quasiparticle loss. Shielding the device from stray light[11,12] and reducing the emissivity of the device should obviously reduce loss. However, to be effective, the shielding needs to protect the device not only from stray light and background blackbody radiation, but also from phonons of energy $> 2\Delta$. Such phonons could be created by the absorption of light in the device, the shielding itself, or in other structures connected to the shields or the device. Enclosing a device in a single aluminum cavity will not necessarily protect the device from phonons generated by light absorbed in the exterior surface of the cavity. Using multiple layers of normal and superconducting shielding should be more effective at thermalizing such high-energy phonons. For example, coating the exterior of a superconducting cavity with low emissivity normal metal (*i.e.* gold) should reduce optical absorption and give better thermalization

of the generated phonons, resulting in fewer high-energy phonons reaching an enclosed device.

Minimizing the kinetic inductance ratio will reduce the sensitivity of loss and frequency shift to temperature changes and optical illumination. On the other hand, for kinetic-inductance detectors it is desirable to increase the frequency shift sensitivity while keeping the loss low. By performing simulations using different material parameters[34], one may be able to identify optimal materials for different purposes. While our simulations reveal that quasiparticle loss decreases when the superconducting gap Δ increases, the kinetic inductance ratio α and characteristic times τ_0, τ_ϕ, and τ_e also affect loss. For example, titanium nitride, with a significantly higher Δ and α compared to Al[50], would be a good candidate for use in kinetic-inductance detectors. The rf power dependent roll-off of quasiparticle loss also depends on the material, and it may be possible to find materials with substantially higher or lower critical power. Finally, the use of quasiparticle traps would reduce the quasiparticle density and its associated loss.

Despite its complexities, we note that our model is still relatively simple in its treatment of optical effects. We believe this approach can be extended to simulate time-dependent behavior and can be improved by using a more complete model of the optical absorption process[36,51].

Appendix: Calculating Quasiparticle Distribution from Kinetic Equations

Following Goldie and Withington[31], the quasiparticle distribution $f(E)$ obeys the kinetic equation[32]

$$
\begin{aligned}
\frac{df(E)}{dt} &= I_{qp}(E, f_r) - \frac{1}{\tau_0(k_B T_c)^3}\left\{ \int_0^\infty d\Omega\, \Omega^2 \right. \\
&\times h_-(E, E+\Omega)\left(f(E)[1-f(E+\Omega)]n(\Omega) \right. \\
&\quad \left. - [1-f(E)]f(E+\Omega)[n(\Omega)+1]\right) \\
&+ \int_0^{E-\Delta} d\Omega\, \Omega^2\, h_-(E, E-\Omega) \\
&\times \left(f(E)[1-f(E-\Omega)][n(\Omega)+1] \right. \\
&\quad \left. - [1-f(E)]f(E-\Omega)n(\Omega)\right)
\end{aligned}
$$

$$
\begin{aligned}
&+ \int_{E+\Delta}^\infty d\Omega\, \Omega^2\, h_+(E, \Omega-E) \\
&\times \left(f(E)f(\Omega-E)[n(\Omega)+1] \right. \\
&\quad \left. - [1-f(E)][1-f(\Omega-E)]n(\Omega)\right)\Bigg\}, \quad \text{(A.1)}
\end{aligned}
$$

Here τ_0 is the characteristic time coefficient for quasiparticle-phonon scattering[47] and T_c is the transition temperature of the superconductor. The term $I_{qp}(E, f_r)$ accounts for excitation of quasiparticles of energy E by a microwave drive at frequency f_r[31,32] where

$$
\begin{aligned}
I_{qp}(E, f_r) &= 2B[h_+(E, E+hf_r)\left(f(E+hf_r)-f(E)\right) \\
&\quad - h_+(E, E-hf_r)\left(f(E)-f(E-hf_r)\right)],
\end{aligned}
\tag{A.2}
$$

The factor B is proportional to rf power at the resonator[31,32], as described further below.

The distribution $n(\Omega)$ of phonons in the superconductor obeys the kinetic equation[31,32]

$$
\begin{aligned}
\frac{dn(\Omega)}{dt} &= \frac{n_{\text{opt}}(\Omega, T_{\text{eff}})}{\tau_e} - \frac{1}{\pi\tau_\phi\Delta}\left\{ 2\int_\Delta^\infty dE\,\rho(E) \right. \\
&\times h_-(E, E+\Omega)\left(f(E)[1-f(E+\Omega)]n(\Omega) \right. \\
&\quad \left. - [1-f(E)]f(E+\Omega)[n(\Omega)+1]\right) \\
&+ \int_\Delta^{\Omega-\Delta} dE\,\rho(E)\, h_+(E, \Omega-E) \\
&\times \left([1-f(E)][1-f(\Omega-E)]n(\Omega) \right. \\
&\quad \left. - f(E)f(\Omega-E)[n(\Omega)+1]\right)\Bigg\} \\
&+ \frac{n_b(\Omega, T_b)-n(\Omega)}{\tau_e}.
\end{aligned}
\tag{A.3}
$$

Here τ_e is the escape time for phonons to leave the superconductor and go into the substrate[37] and τ_ϕ is the characteristic time coefficient for phonon-quasiparticle scattering[47]. The first term on the right hand side is the effective phonon generating source term due to the absorbed optical power P_{opt}. The second term on the right hand side of Eq. (A.3) accounts for phonon-quasiparticle scattering, phonon absorption leading to pair-breaking, and generation of phonons from recombination. The last term accounts for the exchange of phonons with the substrate, which we assume is a thermal phonon bath with a Bose-Einstein distribution $n_b(\Omega, T_b)$ at bath temperature T_b.

To use Eq. (A.2), we need to establish a relationship between the function I_{qp} and the applied rf power P_{rf}, which is our measured independent experimental control parameter. We note that I_{qp} describes the rate at which quasiparticles with energy E are changing occupancy due to the rf drive. We can write the power absorbed by the quasiparticle from the rf drive as[31,32]

$$
P_{\text{rf,ab}} = 4N_0 V \int_\Delta^\infty dE\, I_{\text{qp}}(E, f_r)\, E\, \rho(E). \tag{A.4}
$$

where N_0 is the single-spin density of states at the Fermi surface in the normal state.

Unfortunately $P_{\rm rf}$ and $P_{\rm rf,ab}$ are not equivalent in our apparatus and this complicates the simulation. The power absorbed by quasiparticles $P_{\rm rf,ab}$ is related to the applied rf power $P_{\rm rf}$ by[13]

$$P_{\rm rf,ab} = \frac{2P_{\rm rf}Q^2}{Q_{qp}Q_e}, \qquad (A.5)$$

where Q is the total quality factor of the LC resonator, Q_e is the external quality factor, Q_{qp} is the internal quality factor due to quasiparticles only, and $1/Q = 1/Q_i + 1/Q_e$ [see Eq. (1)]. Notice that to apply Eq. (A.5) and find $P_{\rm rf,ab}$ from $P_{\rm rf}$, we would need to know Q_{qp}, but this is what we want the model to predict. In other words, we need another relation for Q_{qp}. This is provided by Eq. (10).

To find Q_{qp} and $\delta f_r/f_r$, we follow the numerical procedure described by Goldie and Withington[31] and solve Eqs. (A.1), (A.3) and (A.4) for $f(E)$, $n(\Omega)$, and B for the steady state condition $df(E)/dt = 0$ and $dn(\Omega)/dt = 0$. We discretize the problem to evaluate $f(E)$ on 1000 points from $E = \Delta$ to about 7Δ in steps of 1 μeV and $n(\Omega)$ on 1000 points from $\Omega = 0$ to about 6Δ in steps of 1 μeV. Eqs. (A.1), (A.3) and (A.4) yield 2001 simultaneous equations which we then solve using the Newton-Raphson method with $f(E)$, $n(\Omega)$, and B as the solutions.

As input to the simulations, $P_{\rm rf,ab}$ is calculated using Eq. (A.5), with Q_{qp} calculated from Eq. (1). For this step we used the measured values of $P_{\rm rf}$, T_b, $I_{\rm opt}$, Q, Q_i, and Q_e, while Q_0 was a fit parameter and we assumed

$1/Q_{\rm TLS} = 0$. While Δ may depend on temperature, rf drive power, and illumination intensity, for the range of parameters we used the change in Δ was expected to be much smaller than the 1 μeV grid size. Hence we treated Δ as a power- and temperature-independent fit parameter and set $T_c = \Delta/1.76k_B$. We found τ_e by setting $P_{\rm opt}$ in Eq. (5) to agree with Eq. (6) with $\epsilon \approx 15\%$. We used theoretical values[31,47] for τ_0 and τ_ϕ, which satisfy the relation[31]

$$\frac{2\pi N_0\tau_\phi\Delta\Omega_D^3}{9N_i\tau_0(k_BT_c)^3} = 1. \qquad (A.6)$$

Finally, we set f_r in the simulations such that hf_r was the integer multiple of 1 μeV that is closest to measured resonance frequency. Considering that 1 μeV corresponds to a $\approx$ 242 MHz frequency and a 12 mK temperature, the grid size seems coarse. Nevertheless, the solution converges relatively rapidly in about 20 to 30 iterations, and appear well-behaved.

From $f(E)$ we use Eqs. (7), (8), and (10) to find Q_{qp}, then use Eq. (1) to find Q_i. Thus we used the measured value of Q_i as an input to the simulations to calculate, among other values, the simulated value of Q_i. For the equations to be self-consistent, the input and output Q_i values need to be equal. Achieving self-consistency for all $P_{\rm rf}$, $I_{\rm opt}$, and T values requires correct choice of the other parameters. In principle, one could include Eqs. (10) and (A.5) with Eqs. (A.1), (A.3) and (A.4) in the simultaneous solution of equations. This would result in Q_i not explicitly appearing in the simulation. However, this would not alter the result but would increase the complexity of the equations, especially the Jacobian which is needed in the Newton-Raphson method.

* Email: rbudoyo@umd.edu
† Present address: IBM T.J. Watson Research Center, Yorktown Heights, NY 10598, USA
‡ Present address: Agency for Defense Development, Yuseong, Daejeon 305-600, South Korea
1 A. Wallraff, D. I. Schuster, A. Blais, L. Frunzio, R. S. Huang, J. Majer, S. Kumar, S. M. Girvin, and R. J. Schoelkopf, Nature **431**, 162 (2004).
2 M. A. Sillanpaa, J. I. Park, and R. W. Simmonds, Nature **449**, 438 (2007).
3 J. Gao, M. Daal, A. Vayonakis, S. Kumar, J. Zmuidzinas, B. Sadoulet, B. A. Mazin, P. K. Day, and H. G. Leduc, Appl. Phys. Lett. **92**, 152505 (2008).
4 A. Megrant, C. Neill, R. Barends, B. Chiaro, Y. Chen, L. Feigl, J. Kelly, E. Lucero, M. Mariantoni, P. J. J. O'Malley, D. Sank, A. Vainsencher, J. Wenner, T. C. White, Y. Yin, J. Zhao, C. J. Palmstrøm, J. M. Martinis, and A. N. Cleland, Appl. Phys. Lett. **100**, 113510 (2012).
5 P. K. Day, H. G. LeDuc, B. A. Mazin, A. Vayonakis, and J. Zmuidzinas, Nature **425**, 817 (2003).
6 J. Zmuidzinas, Annu. Rev. Cond. Mat. Phys. **3**, 169 (2012).
7 J. M. Martinis, K. B. Cooper, R. McDermott, M. Steffen, M. Ansmann, K. D. Osborn, K. Cicak, S. Oh, D. P. Pappas, R. W. Simmonds, and C. C. Yu, Phys. Rev. Lett. **95**, 210503 (2005).
8 A. D. O'Connell, M. Ansmann, R. C. Bialczak, M. Hofheinz, N. Katz, E. Lucero, C. McKenney, M. Neeley, H. Wang, E. M. Weig, A. N. Cleland, and J. M. Martinis, Appl. Phys. Lett. **92**, 112903 (2008).
9 J. Gao, J. Zmuidzinas, A. Vayonakis, P. Day, B. Mazin, and H. Leduc, J. Low Temp. Phys. **151**, 557 (2008).
10 R. Barends, J. J. A. Baselmans, S. J. C. Yates, J. R. Gao, J. N. Hovenier, and T. M. Klapwijk, Phys. Rev. Lett. **100**, 257002 (2008).
11 R. Barends, J. Wenner, M. Lenander, Y. Chen, R. C. Bialczak, J. Kelly, E. Lucero, P. O'Malley, M. Mariantoni, D. Sank, H. Wang, T. C. White, Y. Yin, J. Zhao, A. N. Cleland, J. M. Martinis, and J. J. A. Baselmans, Appl. Phys. Lett. **99**, 113507 (2011).
12 A. D. Córcoles, J. M. Chow, J. M. Gambetta, C. Rigetti, J. R. Rozen, G. A. Keefe, M. Beth Rothwell, M. B. Ketchen, and M. Steffen, Appl. Phys. Lett. **99**, 181906 (2011).
13 P. J. de Visser, D. J. Goldie, P. Diener, S. Withington, J. J. A. Baselmans, and T. M. Klapwijk, Phys. Rev. Lett.

112, 047004 (2014).

[14] P. J. de Visser, J. J. A. Baselmans, J. Bueno, N. Llombart, and T. M. Klapwijk, Nature Commun. **5**, 4130 (2014).

[15] P. J. de Visser, S. J. C. Yates, T. Guruswamy, D. J. Goldie, S. Withington, A. Neto, N. Llombart, A. M. Baryshev, T. M. Klapwijk, and J. J. A. Baselmans, Appl. Phys. Lett. **106**, 252602 (2015).

[16] J. Hoffman, J. Grover, Z. Kim, A. Wood, J. Anderson, A. Dragt, M. Hafezi, C. Lobb, L. Orozco, S. Rolston, J. Taylor, C. Vlahacos, and F. Wellstood, Rev. Mex. Fis. S **57**, 1 (2011).

[17] M. Hafezi, Z. Kim, S. L. Rolston, L. A. Orozco, B. L. Lev, and J. M. Taylor, Phys. Rev. A **85**, 020302 (2012).

[18] I. M. Pop, K. Geerlings, G. Catelani, R. J. Schoelkopf, L. I. Glazman, and M. H. Devoret, Nature **508**, 369 (2014).

[19] H. Wang, M. Hofheinz, J. Wenner, M. Ansmann, R. C. Bialczak, M. Lenander, E. Lucero, M. Neeley, A. D. O'Connell, D. Sank, M. Weides, A. N. Cleland, and J. M. Martinis, Appl. Phys. Lett. **95**, 233508 (2009).

[20] U. Vool, I. M. Pop, K. Sliwa, B. Abdo, C. Wang, T. Brecht, Y. Y. Gao, S. Shankar, M. Hatridge, G. Catelani, M. Mirrahimi, L. Frunzio, R. J. Schoelkopf, L. I. Glazman, and M. H. Devoret, Phys. Rev. Lett. **113**, 247001 (2014).

[21] M. D. Reed, L. DiCarlo, B. R. Johnson, L. Sun, D. I. Schuster, L. Frunzio, and R. J. Schoelkopf, Phys. Rev. Lett. **105**, 173601 (2010).

[22] J. M. Chow, A. D. Córcoles, J. M. Gambetta, C. Rigetti, B. R. Johnson, J. A. Smolin, J. R. Rozen, G. A. Keefe, M. B. Rothwell, M. B. Ketchen, and M. Steffen, Phys. Rev. Lett. **107**, 080502 (2011).

[23] H. Paik, D. I. Schuster, L. S. Bishop, G. Kirchmair, G. Catelani, A. P. Sears, B. R. Johnson, M. J. Reagor, L. Frunzio, L. I. Glazman, S. M. Girvin, M. H. Devoret, and R. J. Schoelkopf, Phys. Rev. Lett. **107**, 240501 (2011).

[24] W. A. Phillips, Rep. Prog. Phys. **50**, 1657 (1987).

[25] P. Macha, S. H. W. van der Ploeg, G. Oelsner, E. Il'ichev, H.-G. Meyer, S. Wünsch, and M. Siegel, Appl. Phys. Lett. **96**, 062503 (2010).

[26] M. Khalil, F. Wellstood, and K. Osborn, IEEE Trans. Appl. Supercond. **21**, 879 (2011).

[27] L. Faoro and L. B. Ioffe, Phys. Rev. Lett. **109**, 157005 (2012).

[28] L. Faoro and L. B. Ioffe, Phys. Rev. B **91**, 014201 (2015).

[29] B. Sarabi, *Cavity Quantum Electrodynamics of Nanoscale Two-Level Systems*, Ph.D. thesis, University of Maryland, College Park, MD (2014).

[30] Y. Wang, P. Zhou, L. Wei, H. Li, B. Zhang, M. Zhang, Q. Wei, Y. Fang, and C. Cao, J. Appl. Phys. **114**, 153109 (2013).

[31] D. J. Goldie and S. Withington, Supercond. Sci. Technol. **26**, 015004 (2013).

[32] J.-J. Chang and D. Scalapino, Phys. Rev. B **15**, 2651 (1977).

[33] T. Guruswamy, D. J. Goldie, and S. Withington, Supercond. Sci. Technol. **27**, 055012 (2014).

[34] T. Guruswamy, D. J. Goldie, and S. Withington, Supercond. Sci. Technol. **28**, 054002 (2015).

[35] W. H. Parker, Phys. Rev. B **12**, 3667 (1975).

[36] A. Zehnder, Phys. Rev. B **52**, 12858 (1995).

[37] S. B. Kaplan, J. Low Temp. Phys. **37**, 343 (1979).

[38] D. C. Mattis and J. Bardeen, Phys. Rev. **111**, 412 (1958).

[39] J. Gao, *The Physics of Superconducting Microwave Resonators*, Ph.D. thesis, California Institute of Technology, Pasadena, CA (2008).

[40] R. J. Schoelkopf, P. Wahlgren, A. A. Kozhevnikov, P. Delsing, and D. E. Prober, Science **280**, 1238 (1998).

[41] Z. Kim, B. Suri, V. Zaretskey, S. Novikov, K. D. Osborn, A. Mizel, F. C. Wellstood, and B. S. Palmer, Phys. Rev. Lett. **106**, 120501 (2011).

[42] Z. Kim, C. P. Vlahacos, J. E. Hoffman, J. A. Grover, K. D. Voigt, B. K. Cooper, C. J. Ballard, B. S. Palmer, M. Hafezi, J. M. Taylor, J. R. Anderson, A. J. Dragt, C. J. Lobb, L. A. Orozco, S. L. Rolston, and F. C. Wellstood, AIP Advances **1**, 042107 (2011).

[43] We also installed a second fiber that is visible in Fig. 2(b), pointed at the device parallel to the plane of the chip. However the results presented in this paper used just the fiber with perpendicular illumination.

[44] P. J. de Visser, S. Withington, and D. J. Goldie, J. Appl. Phys. **108**, 114504 (2010).

[45] L. J. Swenson, P. K. Day, B. H. Eom, H. G. Leduc, N. Llombart, C. M. McKenney, O. Noroozian, and J. Zmuidzinas, J. Appl. Phys. **113**, 104501 (2013).

[46] B. Sarabi, A. N. Ramanayaka, A. L. Burin, F. C. Wellstood, and K. D. Osborn, Appl. Phys. Lett. **106**, 172601 (2015).

[47] S. Kaplan, C. Chi, D. Langenberg, J. Chang, S. Jafarey, and D. Scalapino, Phys. Rev. B **14**, 4854 (1976).

[48] J. M. Sage, V. Bolkhovsky, W. D. Oliver, B. Turek, and P. B. Welander, J. Appl. Phys. **109**, 063915 (2011).

[49] A. Rothwarf and B. N. Taylor, Phys. Rev. Lett. **19**, 27 (1967).

[50] M. R. Vissers, J. Gao, D. S. Wisbey, D. A. Hite, C. C. Tsuei, A. D. Corcoles, M. Steffen, and D. P. Pappas, Appl. Phys. Lett. **97**, 232509 (2010).

[51] A. G. Kozorezov, A. F. Volkov, J. K. Wigmore, A. Peacock, A. Poelaert, and R. den Hartog, Phys. Rev. B **61**, 11807 (2000).